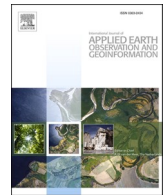




Contents lists available at ScienceDirect

International Journal of Applied Earth Observations and Geoinformation

journal homepage: www.elsevier.com/locate/jag



Temporal connections between long-term Landsat time-series and tree-rings in an urban–rural temperate forest

Mitchell T. Bonney*, Yuhong He

Department of Geography, Geomatics and Environment, University of Toronto Mississauga, 3359 Mississauga Rd, Mississauga, Ontario L5L 1C6, Canada



ARTICLE INFO

Keywords:
Landsat
Time-series
Tree-rings
Dendrochronology
Canopy cover
Segmented regression
Temperate forest

ABSTRACT

Time-series of satellite-derived vegetation proxies and tree-rings widths (TRW) are similar, providing temporal records of forest productivity change from different perspectives and processes. Previous research on this relationship has focused on temperature or moisture limited coniferous forests, using lower spatial resolution (e.g., 8000 m) satellites and normalized difference vegetation index (NDVI) to test relationships over 15–30 years. There is an opportunity to leverage recent advances in building Landsat (30 m) time-series to expand comparisons into new forest types (e.g., coniferous vs. deciduous), areas (e.g., fragmented forests) and over longer periods (e.g., nearly 50 years). However, a better understanding of factors that influence relationship strength is required. We compared tree-ring measurements, converted to a ring width index (RWI), and Landsat tasseled cap angle (TCA) derived canopy cover (CC) from 1972 to 2018 across 16 deciduous, mixed, and coniferous stands in southern Ontario, Canada. For all chronologies, overall relationship strength was assessed with correlation approaches (RWI-CC, both vs. climate), and shorter-term increase-decline trends were compared with segmented regression. There were significant forest type differences, with coniferous chronologies correlating stronger with CC than deciduous. Deciduous chronologies and CC had opposite connections with summer temperature, with climate warming increasing CC and coniferous RWI but not deciduous RWI from 1980 to 2010. More recent decline at most sites appears related to a major ice storm, but multiple factors may be coexisting. We tested the utility of tree-rings for validating nearly 50 years of Landsat-observed change in urban–rural temperate forests, identifying useful connections at coniferous sites. However, there are limitations to comparing long-term Landsat time-series (based on yearly summer data) with annual tree-ring growth.

1. Introduction

Tree-ring widths (TRWs) and remote sensing time-series quantify forest change through time. Trees in temperate and boreal environments grow wood each year, separated into ‘rings’ by a distinctive pattern of earlywood and latewood cells (Speer, 2010). TRW size is influenced by tree age and is dependent on environmental factors around the time of growth, including climate, disturbances, and competition, and is related to net primary productivity or biomass accumulation (Babst et al., 2013). Remote sensing time-series are built from standardized collections of atmospherically corrected imagery which are temporally ‘stacked’, and spectral values are extracted from pixels. Data may be converted to a vegetation index (VI), such as the normalized difference vegetation index (NDVI) based on red and near infrared reflectance, which provides a proxy for forest canopy biomass (Banskota et al., 2014). Therefore, we may expect that TRWs collected from a stand of

trees and VIs from overlapping pixels are correlated and have some structural relationship through time (e.g., Vicente-serrano et al., 2016).

Understanding this relationship is beneficial for those who want to quantify past forest change. There is interest by dendrochronologists, who can use remote sensing to increase the spatial scale of results and link both variables with a limiting factor (e.g., temperature or precipitation). Building connections with remote sensing was recently recognized as a new frontier in tree-ring research (Pearl et al., 2020). There has been less interest by remote sensing scientists, who could benefit from utilizing tree-rings. Advances in building spectrally consistent satellite time-series and change analysis algorithms has inspired the monitoring of gradual forest change and drivers (Rodman et al., 2021), but it is more difficult to know if these changes are ‘real’ and corresponding to forest productivity change (e.g., canopy cover loss) or ‘fake’ and due to the systematic influence of different sensors, atmospheric effects, seasonality, or other noise. There is thus an opportunity to use

* Corresponding author.

E-mail addresses: mitchell.bonney@mail.utoronto.ca (M.T. Bonney), yuhong.he@utoronto.ca (Y. He).

TRW as a natural validation tool for gradual forest change observed by remote sensing, especially if the spectral data are connected to some ecological variable (e.g., canopy cover), since they both measure an aspect of forest productivity at a relatable temporal resolution.

Previous research has focused on temperature or moisture-limited coniferous forest, such as boreal forests (Beck et al., 2011), inner East Asia (Zhou et al., 2020), the Mediterranean (Coulthard et al., 2017), or western North America (Xu et al., 2019). Less research has occurred in temperate mixed or deciduous forest where no one factor clearly limits growth. A recent study identified mixed connections between TRW, VIs, and climate, but shared declines during disturbance events (e.g., ice storms) in Slovenian deciduous forests (Decuyper et al., 2020). There have also been broader scale studies incorporating both forest types, but results have been mixed with some finding that coniferous TRW relate more with VIs than deciduous (Bhuyan et al., 2017; Kaufmann et al., 2008), and others identifying complicated connections involving forest type, climate, and other variables (Vicente-Serrano et al., 2016).

Previous research linking remote sensing with dendrochronology has mostly used low spatial resolution (e.g., 8000 m), but temporally dense, NDVI time-series. The low spatial resolution leads to a well-documented spatial disconnect with tree-ring chronologies (Babst et al., 2018), which may weaken the relationship (Brehaut and Danby, 2018). However, the temporal density of these measurements allows for monthly comparisons between tree-rings, VIs, and climate. Across many different environments, TRW relates most consistently with current summer VIs (e.g., Bhuyan et al., 2017; Xu et al., 2019; Zhou et al., 2020), with some exceptions (Correa-Díaz et al., 2019; Coulthard et al., 2017). NDVI is useful and commonly used, but there is evidence of saturation in high-biomass settings where it becomes increasingly insensitive to further biomass increase (Bonney et al., 2018). Few studies have compared tree-rings with higher spatial resolution sensors (e.g., 30 m Landsat) and tested VIs that incorporate additional bands (e.g., shortwave infrared) to reduce saturation (Sangüesa-Barreda et al., 2014).

There is thus an opportunity to utilize the benefits provided by Landsat time-series to conduct comparisons with tree-rings in an understudied forest setting. Landsat's high spatial resolution means it can isolate the forest change signal in compact or irregularly shaped stands (Babst et al., 2010; Dorman et al., 2015), where the larger pixels of other sensors would include non-forest noise. We can also reduce the spatial disconnect with tree-rings at this scale, such as by sampling the bulk of canopy-dominant trees within a pixel. Furthermore, comparisons have not occurred in urban forests or remnant patches within human-dominated landscapes, even though these forests provide important ecosystem services and more direct societal benefit (Roy et al., 2012). Geographically, we did not locate any relevant studies in the broadleaf and mixed forests of eastern North America where comparisons could be conducted across a diverse forest landscape.

Recent advances in Landsat time-series building also allow for a longer period of overlap with tree-rings than previous comparisons. To this point, 33 years (1981–2013) is the longest overlap period analyzed (Tei and Sugimoto, 2018; Vicente-Serrano et al., 2016) with most studies having 15–30 years of overlap. Efforts to incorporate the Landsat Multispectral Scanner (MSS) into the Landsat time-series framework would extend the record back to 1972 (Pflugmacher et al., 2012), nearing 50 years of overlap and supporting more robust statistical analysis (Pearl et al., 2020). Automated workflows (e.g., LandsatLinkr) have been developed to process large numbers of images to build spectrally and spatially consistent, cloud-free VI time-series across all Landsat sensors (Braaten et al., 2017), and applied to quantify long-term changes in forest canopy cover (Vogeler et al., 2018). However, Landsat's lower temporal resolution combined with cloudy data loss limits these long-term approaches to yearly summer time-series when canopy biomass is relatively stable for multiple satellite overpasses. Nevertheless, this approach would be an advancement over previous Landsat-based comparisons, which have had many missing 'no-data' years (Sangüesa-Barreda et al., 2014).

More consideration should be given to VIs that incorporate additional wavelengths, such as tasseled cap (TC) transformations that incorporate blue, green, red, near infrared, and shortwave infrared at different weights (Crist, 1985). Tasseled cap angle (TCA), based on the arctan of TC greenness divided by TC brightness, is a proxy for the percentage of vegetation to non-vegetation and has the capability to distinguish between densities of forest cover (Ahmed et al., 2014; Powell et al., 2010). TCA correlates strongly with the more commonly used NDVI ($r = 0.97$) but is less impacted by high-biomass saturation (Ma et al., 2018), which may be important in dense temperate forest canopies. Furthermore, the LandsatLinkr process is based on TC indices (Braaten et al., 2017). Understanding how this type of VI and time-series process (i.e., yearly summer observations) relate with annual tree-ring growth, including potential limitations (e.g., seasonal disconnects in response to limiting factors like climate), is vital for advancing TRW-remote sensing comparisons over longer periods and to new forest settings.

In this study, we compare TRWs collected at 16 temperate forest sites across an urban–rural watershed in Canada to overlapping Landsat TCA-based percent canopy cover (CC) from 1972 to 2018. We combine recent advances in long-term Landsat time-series building and dendrochronology to formulate new temporal connections in an understudied forest setting. The objectives were to (1) quantify the strength of the relationship between TRW and CC across a diverse forest landscape; (2) understand how certain factors (i.e., forest type, landscape setting, monthly climate) influence relationships; and (3) compare the temporal structure (e.g., increase-decline trends) of TRW and CC to identify time-periods of agreement or disagreement and infer drivers (e.g., disturbances). We aim to better understand the utility of long-term Landsat summer time-series for comparison with annual tree-rings and test the potential of TRW as a validation tool in temperate forest settings.

2. Methods

2.1. Study area

This study focuses on the Credit River Watershed (CRW), located west of Toronto in southern Ontario, Canada (Fig. 1). The southern portion includes the suburban cities of Mississauga and Brampton, with Orangeville and more rural towns in the north and west. The CRW is at the boundary of the Great Lakes St. Lawrence mixed forest and Carolinian deciduous forest regions. According to the most recent Ecological Land Classification (ELC) (CVC, 2019), about 25% of the CRW is forest. Half (52%) is deciduous, mostly maple (*Acer spp.*), although ash (*Fraxinus spp.*), oak (*Quercus spp.*), beech (*Fagus spp.*), birch (*Betula spp.*), hickory (*Carya spp.*), hop hornbeam (*Ostrya spp.*), cherry (*Prunus spp.*), basswood (*Tilia spp.*) and poplar (*Populus spp.*) are also common. About 30% is coniferous, including cedar (*Thuja spp.*), hemlock (*Tsuga spp.*), pine (*Pinus spp.*), spruce (*Picea spp.*) and fir (*Abies spp.*). Drier forests are maple dominated, while ash and poplar have been majorities in swamps. Ash trees have been in decline since emerald ash borer (EAB) spread here in 2008 (Mississauga Parks and Forestry, 2020). The most extensive coniferous stands are plantations (usually pine or spruce). Natural cedar-dominated stands are common, especially in wetter areas, while other coniferous species are mostly found in mixed stands (18% of forests). In urban areas, forest cover is low and fragmented with patches found in city parks and along the Credit River. In rural areas, forest cover is higher, with patches interspersed between farmland and in a corridor along the Niagara Escarpment.

The CRW has a humid continental climate that has been impacted by climate change (Fig. 2). The mean annual temperature (1940–2018) is 8.1 °C, with warm summers (20–25 °C) and cold winters (below 0 °C). Temperatures have increased by almost 2 °C since 1970. The mean annual total precipitation (1940–2018) is 867 mm that is evenly distributed from month-to-month on average. Precipitation has fluctuated, with notable wet periods from 1974 to 1985, 1992–1995, and

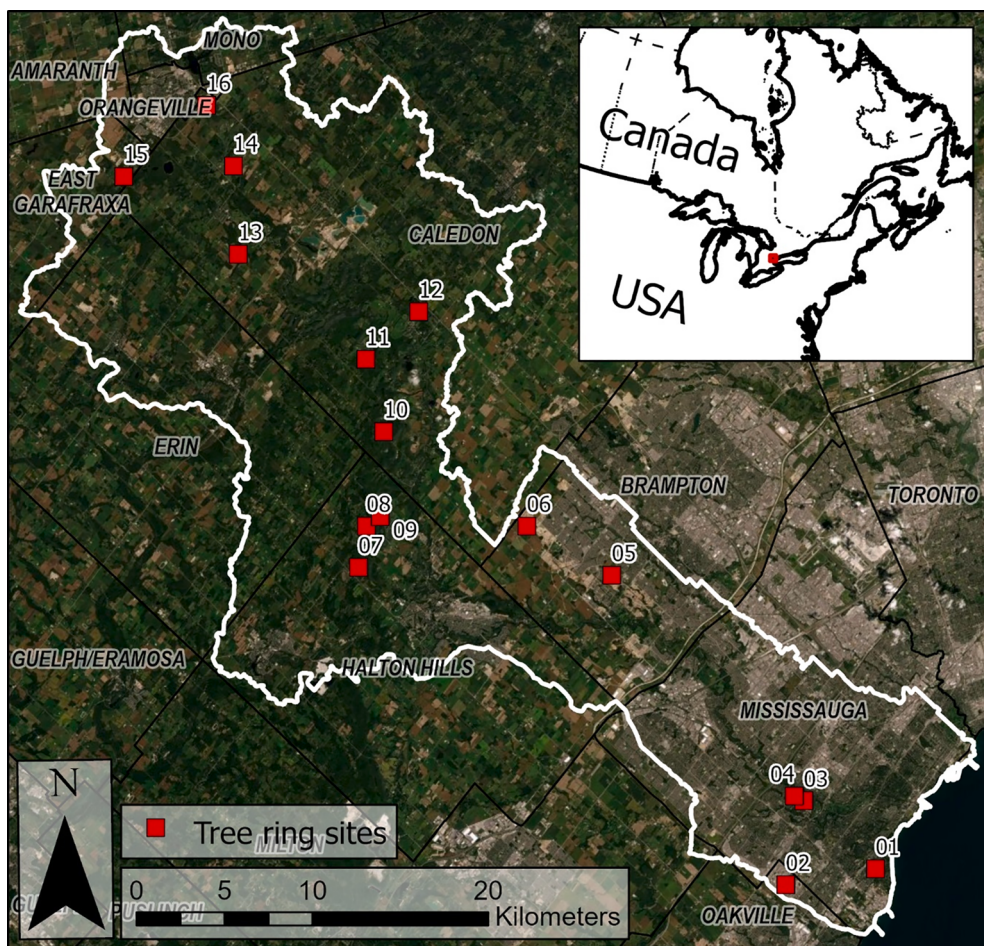


Fig. 1. Credit River Watershed (white) in southern Ontario, Canada. Basemap is from ArcGIS Pro, dated to summer 2018.

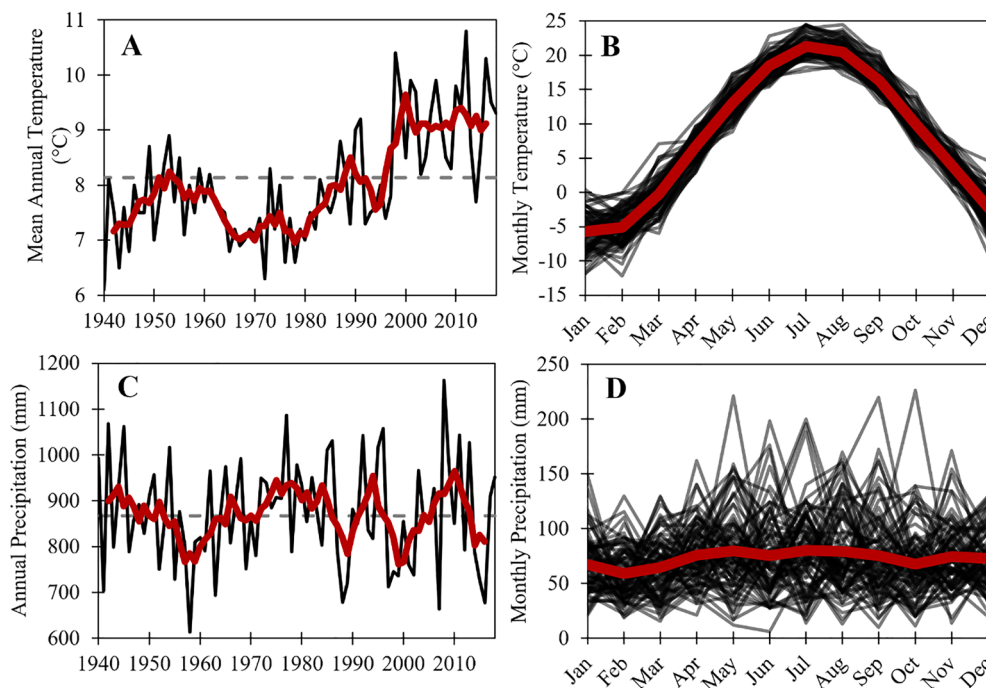


Fig. 2. Local climate from 1940 to 2018 from adjusted and harmonized Canadian climate data (Mekis and Vincent, 2011; Vincent et al., 2020) collected at Pearson Airport ($79^{\circ}37'48''W$, $43^{\circ}40'48''N$). Mean annual temperature (A) and total precipitation (C) include black lines for yearly values, red lines for five year running means and gray dashed lines for the 1940–2018 average. Monthly mean temperature (B) and total precipitation (D) include black lines for yearly by-month values and red lines for the 1940–2018 by-month average. (For interpretation of the references to color in this figure legend, the reader is referred to the web version of this article.)

2006–2012.

2.2. Building Landsat time-series

To build the longest-possible remote sensing time-series, Landsat images from the entirety of the archive (1972–2018) were evaluated. In total, 315 images overlapping the CRW were downloaded from the USGS EarthExplorer (<http://ear�explorer.usgs.gov/>) and included (Table A1). All Landsat sensors were included: MSS from Landsat 1–5, TM from Landsat 4–5, ETM+ from Landsat 7, and OLI from Landsat 8. Images date between Julian day 160 (June 9 in a non-leap year) and 240 (August 28) to minimize spectral differences due to seasonality (Fig. 2b) while maximizing cloud-free data potential. TM, ETM+, and OLI images are Landsat Collection 1 Level-2, converted to surface reflectance with the LEDAPS algorithm (Masek et al., 2006) for TM/ETM+ and with LaSRC (Vermote et al., 2016) for OLI. MSS images are Landsat Collection 1 Level-1 with precision terrain correction (L1TP).

Images were made spectrally and spatially consistent and converted to a yearly composite time-series with LandsatLinkr, which is designed to work with summer images (Braaten et al., 2017; Vogeler et al., 2018). This is a six-step process in R (R Core Team, 2013) that 1) prepares MSS imagery by unpacking, resampling (60 m to 30 m), reprojecting, improving georegistration, converting to surface reflectance, and masking clouds and shadows (Braaten et al., 2015; Chavez, 1996, 1988; Kennedy and Cohen, 2003). 2) TM/ETM+ imagery is prepared by unpacking, reprojecting, applying tasseled cap (TC) transformations (including TCA), and masking clouds with Fmask (Crist, 1985; Powell et al., 2010; Zhu et al., 2015). 3) OLI imagery is prepared with a similar process as TM/ETM+, but without TC transformations. 4) MSS imagery is spectrally calibrated to TM, and modeled TC indices are created based on coincident images collected between 1984 and 1994 (Pflugmacher et al., 2012). 5) OLI imagery is spectrally calibrated to ETM+ with a similar process based on near-date images between 2013 and 2018. TM and ETM+ are nearly identical sensors and do not require calibration to each other. 6) Annual median summer TC image composites are created at the pixel level by combining all available values each year and removing values associated with clouds or no data (i.e., ETM + SLC-off) (Pflugmacher et al., 2012). For more details on the LandsatLinkr process, see Braaten et al. (2017) and Vogeler et al. (2018).

A random inspection of sample pixels showed that time-series were not systematically influenced by changes in Landsat sensors (e.g., TM added to MSS in 1984), with no structural change in TCA during sensor transition periods across land covers (Fig. A1). However, we identified residual atmospheric influence in select years with less available cloud-free data (e.g., 1988). Any year with no available value or an atmospheric outlier (e.g., ephemeral large decline in VI value) were recalculated as the average from the year before and after or replaced with a more representative single-date image value from that summer if available. Across all sites, 3.5% of years had no available value and 6% of years were influenced by atmospheric effects. The most impacted years were 1973 (100% of sites, no available images), 1977 (25%), 1988 (38%), 1998 (44%), and 2003 (31%). For this study, we extracted average TC time-series for 3x3 pixel windows centered on tree-ring sites (Fig. 3) for further analysis.

To connect the Landsat TC time-series to an ecological variable, we built a linear relationship between 2018 TC data and percent CC derived from hemispherical photographs (Leblanc, 2008) collected at these and other CRW forest sites (Fig. A2). We selected TCA for comparison with tree-rings because it related more strongly to CC than other tested VIs while being highly correlated to the more commonly used NDVI ($r = 0.95^{***}$; Ma et al., 2018). Using this relationship and assuming it remained consistent through time, we converted our time-series from TCA to CC.

2.3. Building tree-ring chronologies

We visited 16 forest sites (Fig. 3) in summer 2019 to collect tree-rings and build chronologies for comparison with the Landsat-derived CC time-series. These sites were selected with the goal of visiting a diverse set of forest types (i.e., deciduous, coniferous, mixed; forest, swamp, plantation) and settings (i.e., urban, rural). At each site, we collected cores from all canopy-dominant trees within approximately 20 m of the center point of the 3×3 Landsat pixel window (Fig. 3) that had a diameter at breast height (DBH) of at least 20 cm, with the goal of coring 20–30 trees per site. Two cores were collected from each tree at perpendicular angles. Cores were prepared for TRW measurement with standard dendrochronology methods (Speer, 2010). Cores were scanned at 2400 dpi with an EPSON Perfection V850 Pro.

TRW was measured to the nearest 0.001 mm in CooRecorder (Larsson, 2019). Core series from a tree were compared to identify mistakes or false/missing rings. Correlations between these series were generally high (0.71 ± 0.11), indicating robust tree-level dating. To facilitate consistent tree-to-tree dating, narrow marker years were identified. Once all series from a site had been measured and confirmed, preliminary chronologies were created in CDendro (Larsson, 2019). Multiple TRW chronologies were created for some sites depending on forest composition. Chronologies were only built if at least nine trees and 15 cores were included. Preliminary chronologies were crossdated using dplR (Bunn, 2010, 2008) in R. The corr.rwl.seg command with 20-year segments was used to test the correlation of each series with the rest of the chronology through time. Segments that did not significantly correlate ($p > 0.05$) with the master chronology were identified and those series were inspected statistically with dplR and visually in CooRecorder. Series that could not be effectively crossdated with the rest of the chronology were removed. From the 16 sites, we created 20 crossdated TRW chronologies using Tukey's biweight robust mean (Table 1).

2.4. Relating tree-rings with Landsat time-series

To compare tree-ring chronologies, they should be detrended and standardized from TRW (mm) to a unitless ring width index (RWI). We tested different detrending methods (Spline, ModNegExp, Mean, Ar, Friedman, ModHugershoff) in dplR (Bunn, 2008), and found that standard ModNegExp detrended TRW provided the strongest correlations with TCA-based CC time-series. ModNegExp corrects for age-related growth trends (i.e., younger trees grow wider rings) by fitting a negative exponential curve (Fritts, 2001). RWI chronologies were truncated based on subsample signal strength, with only years ≥ 0.85 included (Buras, 2017; Wigley et al., 1984).

In R, we used Pearson's correlation (one-sided, greater) to quantify the strength and significance ($p < 0.05$) of relationships between RWI and CC (1972–2018) for each chronology. Since there is some evidence of a temporal lag between canopy and tree-ring width increase (Bhuyan et al., 2017), we also correlated RWI chronologies with CC time-series from the previous year. When comparing non-residual time-series, we are aware that correlation assumes statistical independence and that this is not the case if there is significant year-to-year autocorrelation ($p < 0.05$). Therefore, for all time-series correlations reported in this study we used a modified cor.test function that penalizes significance by reducing effective sample size (N_{eff}) in proportion to the strength of the autocorrelation whenever an autocorrelated time-series was included (Berner et al., 2011; Dawdy and Matalas, 1964).

To elucidate seasonal climate-based limiting factors between RWI and CC, we correlated RWI and CC time-series (1972–2018) for all chronologies with monthly mean temperature and total monthly precipitation time-series from the same and previous year (e.g., Coulthard et al., 2017). For temperature, we considered the monthly mean of daily mean, minimum, and maximum, but present results only for daily mean because interpretations did not notably differ and they were strongly



Fig. 3. Tree-ring sites (Fig. 1), showing the surrounding landscape around each Landsat pixel window and tree-ring collection area, and ground-level photographs (including latitude and longitude). Dec: deciduous, Con: coniferous. See Table 1 for details. Forest type based on CVC ELC (CVC, 2019). Background 50 cm resolution leaf-off aerial photograph was collected by CVC in spring 2013. The areas surrounding sites 05 and 06 have been developed since photograph collection.

Table 1

Tree-ring chronology information. Chronologies ordered by site and labeled based on their core composition: Dec (deciduous mix), Ace (*Acer*), Car (*Carya*), Que (*Quercus*), Bet (*Betula*), Pop (*Populus*), Pic (*Picea*), Thu (*Thuja*), Tsu (*Tsuga*), Pin (*Pinus*). Forest type of chronology (coniferous: Con, deciduous: Dec) shown in parentheses. First year is the earliest ring recorded. All chronologies end in 2018. AR1 is first order autocorrelation. EPS is expressed population signal (Wigley et al., 1984).

Chronologies by site	# Trees (Cores)	Core Composition	First year	Age (years)	Ring widths (mm)	Series inter-correlation	AR1	EPS
01Tsu (Con)	10 (19)	Tsuga (19)	1868	114 ± 15	1.1 ± 0.3	0.56 ± 0.10	0.83 ± 0.08	0.86
02Ace (Dec)	9 (18)	Acer (18)	1892	110 ± 12	0.9 ± 0.2	0.64 ± 0.07	0.64 ± 0.17	0.90
02Que (Dec)	12 (23)	Quercus (23)	1898	101 ± 26	1.5 ± 0.4	0.65 ± 0.06	0.69 ± 0.09	0.91
03Ace (Dec)	14 (27)	Acer (27)	1897	111 ± 11	1.1 ± 0.4	0.66 ± 0.07	0.56 ± 0.13	0.94
03Que (Dec)	12 (24)	Quercus (24)	1898	103 ± 11	2.0 ± 0.4	0.74 ± 0.05	0.77 ± 0.08	0.95
04Tsu (Con)	16 (30)	Tsuga (30)	1880	114 ± 19	1.1 ± 0.4	0.61 ± 0.04	0.76 ± 0.10	0.93
05Ace (Dec)	23 (42)	Acer (42)	1877	104 ± 25	1.0 ± 0.5	0.65 ± 0.09	0.65 ± 0.09	0.94
06Dec (Dec)	14 (28)	Acer (20), Carya (2), Prunus (2), Tilia (4)	1907	87 ± 21	1.8 ± 0.7	0.63 ± 0.09	0.71 ± 0.11	0.91
07Thu (Con)	29 (57)	Thuja (57)	1903	74 ± 17	1.5 ± 0.3	0.61 ± 0.07	0.69 ± 0.16	0.95
08Ace (Dec)	16 (31)	Acer (31)	1933	70 ± 8	1.7 ± 0.6	0.69 ± 0.08	0.55 ± 0.12	0.94
09Pin (Con)	28 (53)	Pinus (53)	1979	35 ± 3	3.6 ± 0.8	0.66 ± 0.12	0.80 ± 0.10	0.96
10Dec (Dec)	11 (20)	Acer (14), Betula (3), Carya (2), Tilia (1)	1891	91 ± 14	1.3 ± 0.2	0.73 ± 0.12	0.51 ± 0.17	0.93
10Thu (Con)	16 (31)	Thuja (31)	1902	105 ± 10	1.0 ± 0.2	0.69 ± 0.07	0.76 ± 0.08	0.96
11Ace (Dec)	28 (53)	Acer (53)	1929	70 ± 9	1.6 ± 0.3	0.64 ± 0.08	0.67 ± 0.10	0.96
12Pop (Dec)	12 (21)	Populus (21)	1944	62 ± 11	2.3 ± 0.5	0.48 ± 0.07	0.59 ± 0.15	0.83
13Pic (Con)	21 (41)	Picea (41)	1956	56 ± 5	2.7 ± 0.7	0.60 ± 0.07	0.70 ± 0.19	0.94
14Thu (Con)	22 (43)	Thuja (43)	1922	72 ± 11	1.7 ± 0.6	0.63 ± 0.09	0.63 ± 0.15	0.95
15Ace (Dec)	9 (15)	Acer (15)	1933	74 ± 9	1.8 ± 0.2	0.61 ± 0.08	0.89 ± 0.02	0.88
15Bet (Dec)	10 (17)	Betula (17)	1940	74 ± 5	1.4 ± 0.2	0.58 ± 0.11	0.69 ± 0.09	0.88
16Thu (Con)	30 (60)	Thuja (60)	1920	74 ± 8	1.6 ± 0.3	0.69 ± 0.07	0.79 ± 0.08	0.98

related (i.e., monthly $R^2 \approx 0.90$ for mean vs. minimum or maximum). We used Pearson correlation (two-sided) with autocorrelation corrections. Months from previous-year May to same-year September were included. For all sites, the closest station with adjusted and homogenized Canadian climate data (Mekis and Vincent, 2011; Vincent et al., 2020) for both temperature and precipitation dating back to 1971 was Pearson Airport (Fig. 2). Sites are located between 13 and 46 kms from the station.

To quantify increase-decline dynamics through time, we fit RWI and CC time-series into a segmented regression framework in R. For each time-series a simple linear model was built, from which the most appropriate number of breakpoints and their estimated year was identified based on the model with the lowest Bayesian information criterion and incorporating the Davies' and pseudo score tests (Davies, 2002; Muggeo, 2020, 2008). This breaks the time-series into segments, and we calculated Theil-Sen slope (TS) and Mann-Kendal significance (MK) for each segment. TS, which is nonparametric and robust to outliers, finds the median of slopes for all pair-wise iterations (Sen, 1968; Theil, 1950) and can be plotted by also including the estimated intercept (Bronaugh and Werner, 2019). The MK test determines if TS trends are significant ($p < 0.05$), and therefore clearly increasing (i.e., RWI or CC gain) or declining (i.e., RWI or CC loss) (Kendall, 1975; Mann, 1945). As above, we used a modified MK test that reduces N_{eff} for autocorrelated segments when calculating trend significance (Hamed and Rao, 1998;

Patakamuri and O'Brien, 2020). With this framework we converted each RWI chronology and CC time-series into a series of growing, declining or insignificant segments split by statistically defined breakpoints.

3. Results

3.1. Time-series relationships

Nine of 20 chronologies at nine of 16 sites had a significant positive relationship between ModNegExp detrended RWI and TCA-based CC (Fig. 4). The strongest positive correlations were found at an urban hemlock-mixed forest (01Tsu, $r = 0.64^{**}$), a rural poplar-deciduous swamp (12Pop, $r = 0.57^{**}$), and a rural cedar-mixed forest (10Thu, $r = 0.55^*$). For these chronologies, RWI and CC increase from 1980 until 2010, and then begin to decline. The weakest correlations were found at two maple-deciduous forests (11Ace, $r = -0.22$; 05Ace, $r = -0.21$). Spatially, there was no consistent correlation pattern, with significant relationships spread across the CRW and large variations for chronologies at the same site (Fig. 5a).

For all chronologies, the average correlation was 0.16 ± 0.27 for same-year RWI-CC (Fig. 5b). Results with previous-year CC were significantly lower using a paired t -test ($p < 0.05$), with an average correlation of 0.11 ± 0.28 . Therefore, further analysis focuses on same-year CC. There was no difference between sites located in more rural

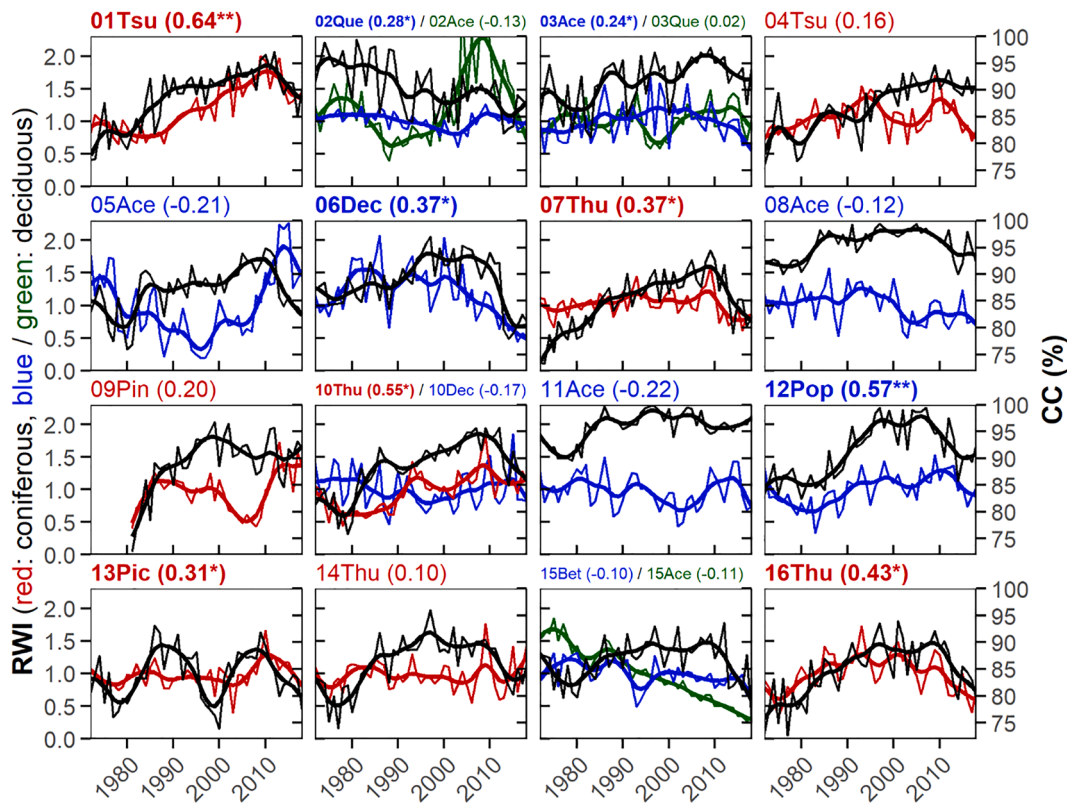


Fig. 4. RWI (left Y-axis) and CC (right Y-axis, black) plotted through time (1972–2018) for all chronologies across 16 sites (Table 1). Coniferous RWI are shown in red and deciduous are shown in blue or green (second deciduous chronology at multi-deciduous sites). Thicker lines are 10-year smoothing splines. RWI-CC correlation, and significance noted above each plot. Significant correlations are in bold, and asterisks indicate p-value ($* \leq 0.05$, $** \leq 0.01$, $*** \leq 0.001$). (For interpretation of the references to color in this figure legend, the reader is referred to the web version of this article.)

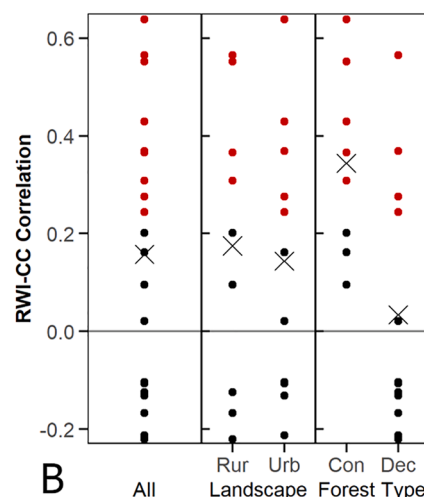
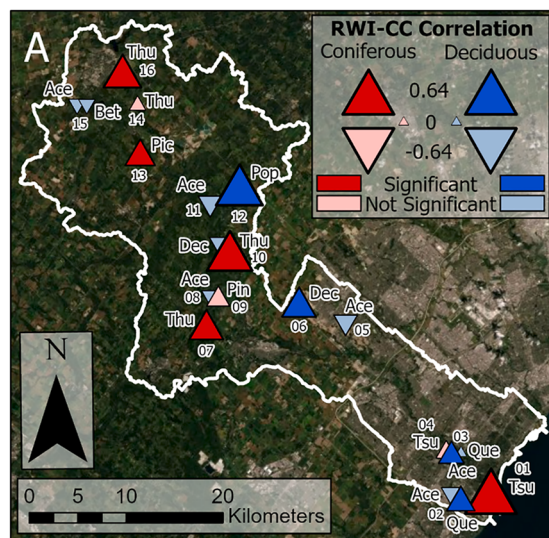


Fig. 5. RWI-CC correlations (1972–2018). A. Map of correlations. Labels indicate site number and genus. Multi-chronology sites (i.e., 02, 03, 10, 15) are shown with offset symbols. B. Plotted correlations: all, rural–urban, coniferous–deciduous. Urban sites are those located in Mississauga, Brampton, and on the edge of Orangeville, with other sites being rural. Red points are significant and black points are not. Crosses are averages. (For interpretation of the references to color in this figure legend, the reader is referred to the web version of this article.)

settings ($r = 0.17 \pm 0.28$) and those in more urban settings ($r = 0.14 \pm 0.26$). However, there were significant differences based on forest type (t-test, $p < 0.05$), with coniferous chronologies ($r = 0.35 \pm 0.18$) correlating stronger than deciduous ($r = 0.03 \pm 0.25$). Maple chronologies were notably low ($r = -0.09 \pm 0.16$), and all but one correlation with CC was negative. There was no significant connection with RWI-CC correlation along gradients of dendrochronological statistics (e.g., series inter-correlation, Table 1) or forest density variables collected during fieldwork (i.e., CC, stem density, basal area) (Fig. A3).

3.2. Connections with climate

RWI and CC varied in correlation with temperature seasonally and by forest type. Across all months, coniferous RWI correlated more positively than deciduous (Fig. 6a). Most (82%) significant positive correlations were coniferous, while most (89%) significant negative correlations were deciduous. Coniferous RWI correlated most with spring temperature (April $r = 0.22 \pm 0.13$, 38% significantly positive), meaning that warmer springs were weakly associated with wider

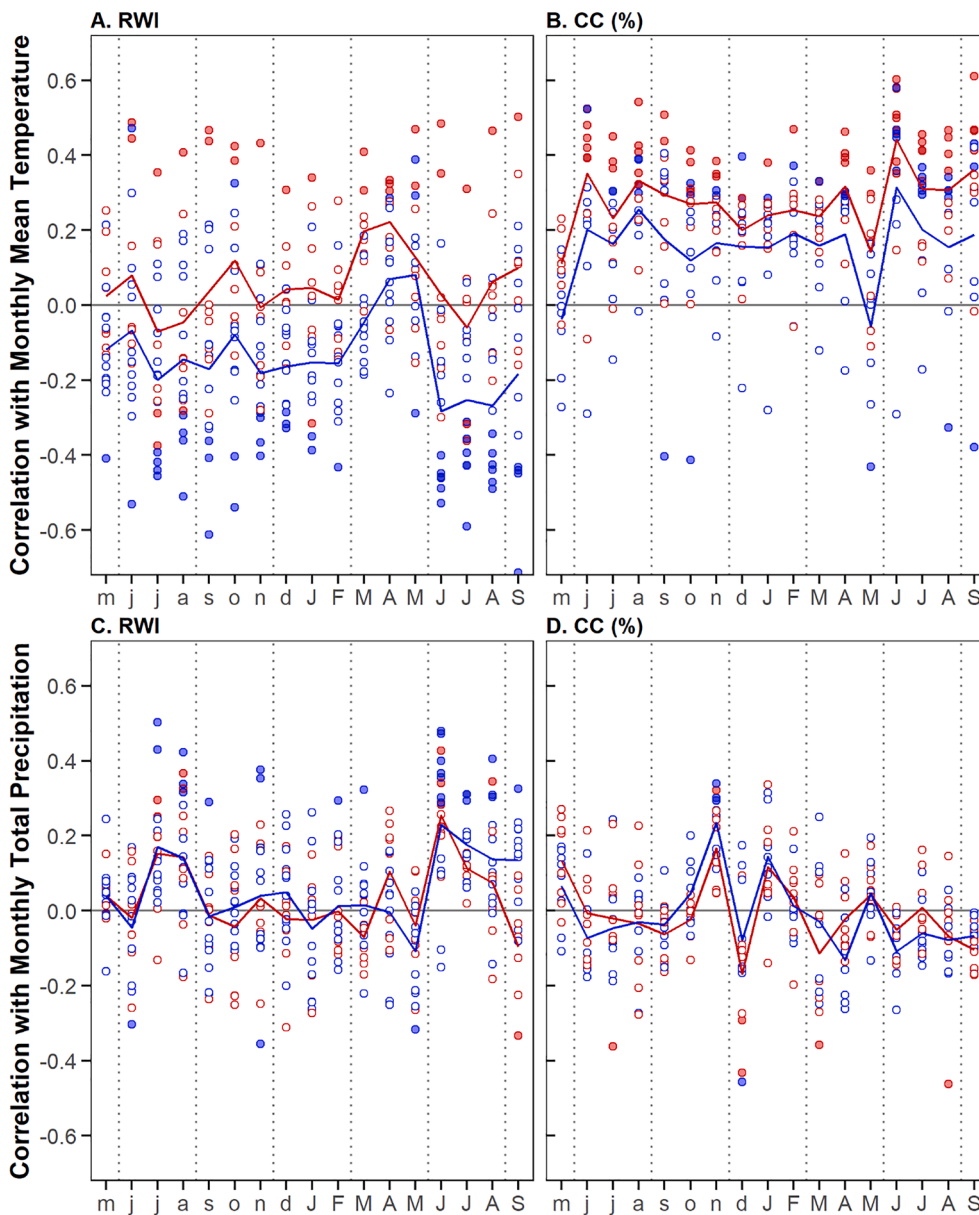


Fig. 6. RWI and CC (1972–2018) correlation with adjusted and homogenized monthly mean of the daily mean temperature and total monthly precipitation (Mekis and Vincent, 2011; Vincent et al., 2020) over the same period (Fig. 2) from previous May (m) to current September (S). Vertical dotted lines separate seasons. RWI and CC split into coniferous (red) and deciduous (blue) chronologies. Filled points represent significant correlations. Lines represent forest type averages. See Figs. A4 and A5 for temperature and precipitation correlations at individual sites and chronologies. (For interpretation of the references to color in this figure legend, the reader is referred to the web version of this article.)

coniferous TRW. Spring was also the only season where the average deciduous RWI correlation was positive. Deciduous RWI correlated most with mean summer temperature (June-August $r = -0.32 \pm 0.22$, 50% significantly negative), meaning that warmer summers were moderately associated with narrower deciduous TRW. Coniferous RWI had no correlation with summer temperature on average. Both coniferous and deciduous chronology CC correlated positively with temperature in almost every month (i.e., warmer temperatures were associated with higher CC), but coniferous correlations were always more positive than deciduous on average (Fig. 6b). Most (61%) significant positive correlations were coniferous. The strongest correlations occurred in June for both coniferous ($r = 0.44 \pm 0.15$, 88% significantly positive) and deciduous ($r = 0.31 \pm 0.27$, 63% significantly positive) CC.

RWI and CC varied in correlation with precipitation seasonally, but not by forest type. RWI correlated most with total summer precipitation (June-August $r = 0.30 \pm 0.16$, 60% significantly positive), meaning that wetter summers were moderately associated with wider TRW (Fig. 6c). Correlations were also weakly positive with previous-July/August precipitation. All other months had no correlation on average. Except for contrasting weakly positive and negative correlations during previous-

November/December, CC and precipitation did not correlate with most months averaging close to zero correlation and few significant points (Fig. 6d). Coniferous and deciduous chronologies followed similar correlation patterns for both RWI and CC.

3.3. Increase-decline trends

Segmented regression revealed similar patterns of increase-decline across individual chronologies and Landsat time-series (Fig. 7), but RWI and CC trends in overlap years (1972–2018) were more consistent for coniferous chronologies. Although input coniferous RWI and CC were noisy across sites, they increased on average from 1980 until around 2010 when both began to decline (Fig. 8a). Deciduous RWI was more stable during this period, even though overlapping CC time-series followed similar, but less pronounced, trends as coniferous CC. Average coniferous RWI and CC had a positive and significant correlation ($r = 0.56^{**}$) while deciduous RWI and CC had a negative correlation ($r = -0.27$). Coniferous RWI and CC breakpoints reinforced these observations, especially around 2010 where breakpoints for both were most common and generally followed by declining or insignificant trends

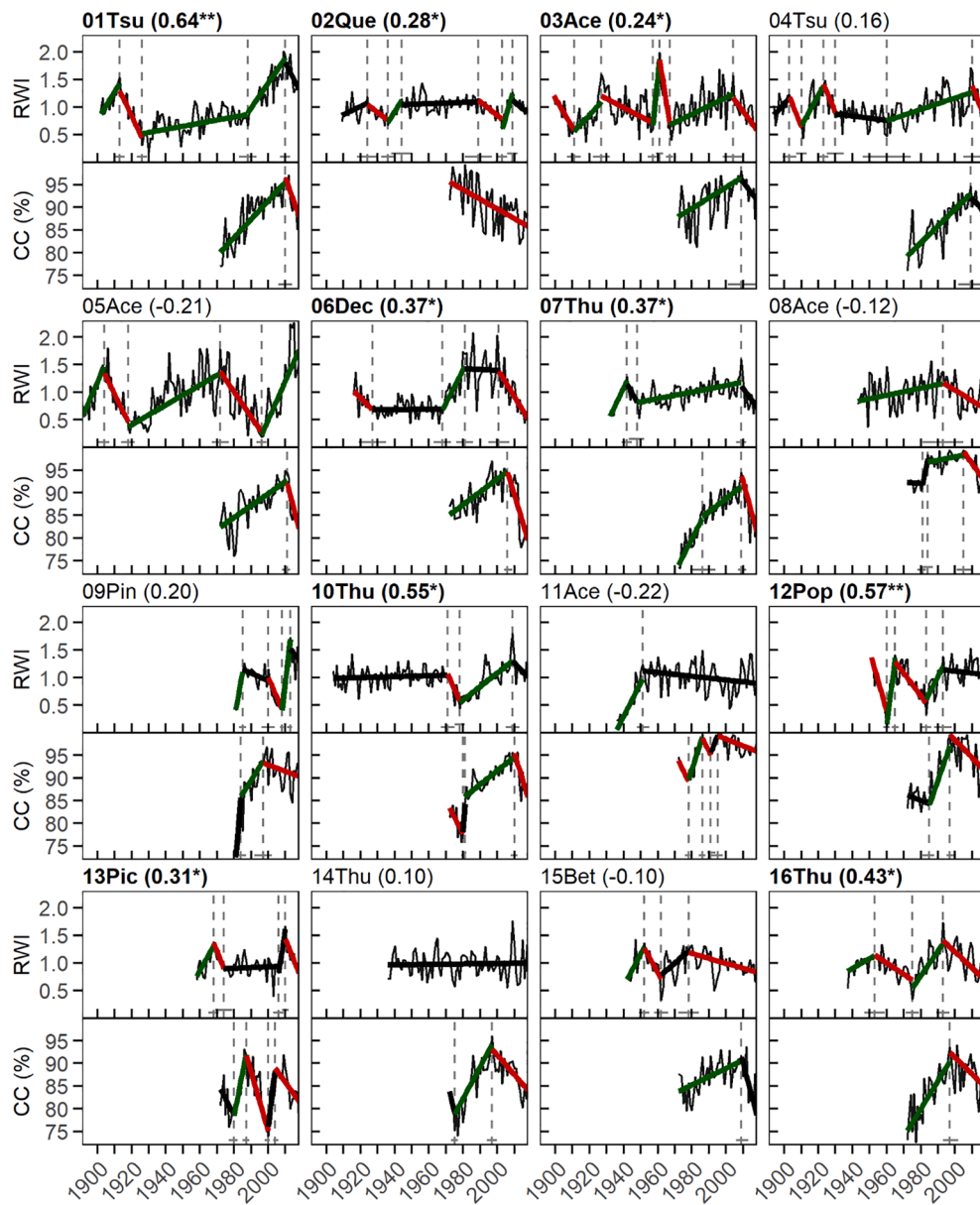


Fig. 7. RWI and CC increase-decline trends built with segmented regression. Green segments are significantly increasing, red segments are significantly decreasing, and black segments are insignificant. Vertical dashed lines are breakpoint years between segments, accompanied by a standard error line at 95% confidence. Noisy lines are the input RWI and CC time-series from which segments and breakpoints were calculated. See Fig. A6 for second chronologies at sites 02, 03, 10, and 15. (For interpretation of the references to color in this figure legend, the reader is referred to the web version of this article.)

(Fig. 8b). Deciduous RWI and CC breakpoints did not follow a consistent pattern. Coniferous and deciduous CC breakpoints were usually followed by increasing trends in the 1980s and decreasing trends in more recent years.

Coniferous RWI and CC followed similar increase-decline trends throughout their overlap period. Coniferous RWI and CC transitioned from decline to increase in the 1970s, increased in the 1980s (i.e., positive segment slopes), remained relatively stable in the 1990s and 2000s, and declined in the 2010s (i.e., negative segment slopes) (Fig. 8c-d). The only disagreement was in the late 2000s, during the wettest year on record (Fig. 2c), when a spike in RWI increase was not matched by CC. For both RWI and CC, the 1980s represent the longest period of strong and consistent increase on record. In 1983, for example, all RWI and CC slopes are positive (mostly significant) and increasing at rates of $0.033 \text{ RWI yr}^{-1}$ and $1.18\% \text{ CC yr}^{-1}$ (Table 2). Conversely, the 2010s represent the strongest period of decline since the 1920s. By 2018 almost all RWI and CC slopes were negative (often significant, although impacted limited sample size at the end of the time-series) and declining at rates of $-0.045 \text{ RWI yr}^{-1}$ and $-0.68\% \text{ CC yr}^{-1}$.

Deciduous RWI and CC do not follow similar increase-decline trends.

In fact, from 1980 to 2010 segments trend in roughly opposite directions (Fig. 8c-d). In 1983, most RWI slopes were negative ($-0.013 \text{ RWI yr}^{-1}$) while most CC slopes were positive ($0.47\% \text{ CC yr}^{-1}$) (Table 2). As with coniferous, deciduous RWI and CC have declined since 2010, although at slower rates of RWI decline. By 2018, most RWI slopes and all CC slopes were negative, but with deciduous RWI declining slower ($-0.025 \text{ RWI yr}^{-1}$) and deciduous CC declining similarly ($-0.74\% \text{ CC yr}^{-1}$) compared to coniferous. Overall, there was clear agreement between coniferous RWI and CC increase-decline trends that was not matched by deciduous chronologies.

4. Discussion

4.1. Advances in relating remote sensing and tree-rings

In this study, we used long-term Landsat time-series for monitoring forest change and comparing with tree-rings over a common period of 47 years (1972–2018). This is 14 years more than the previous longest comparisons (Tei and Sugimoto, 2018; Vicente-Serrano et al., 2016), providing a larger sample size for correlation analyses and the

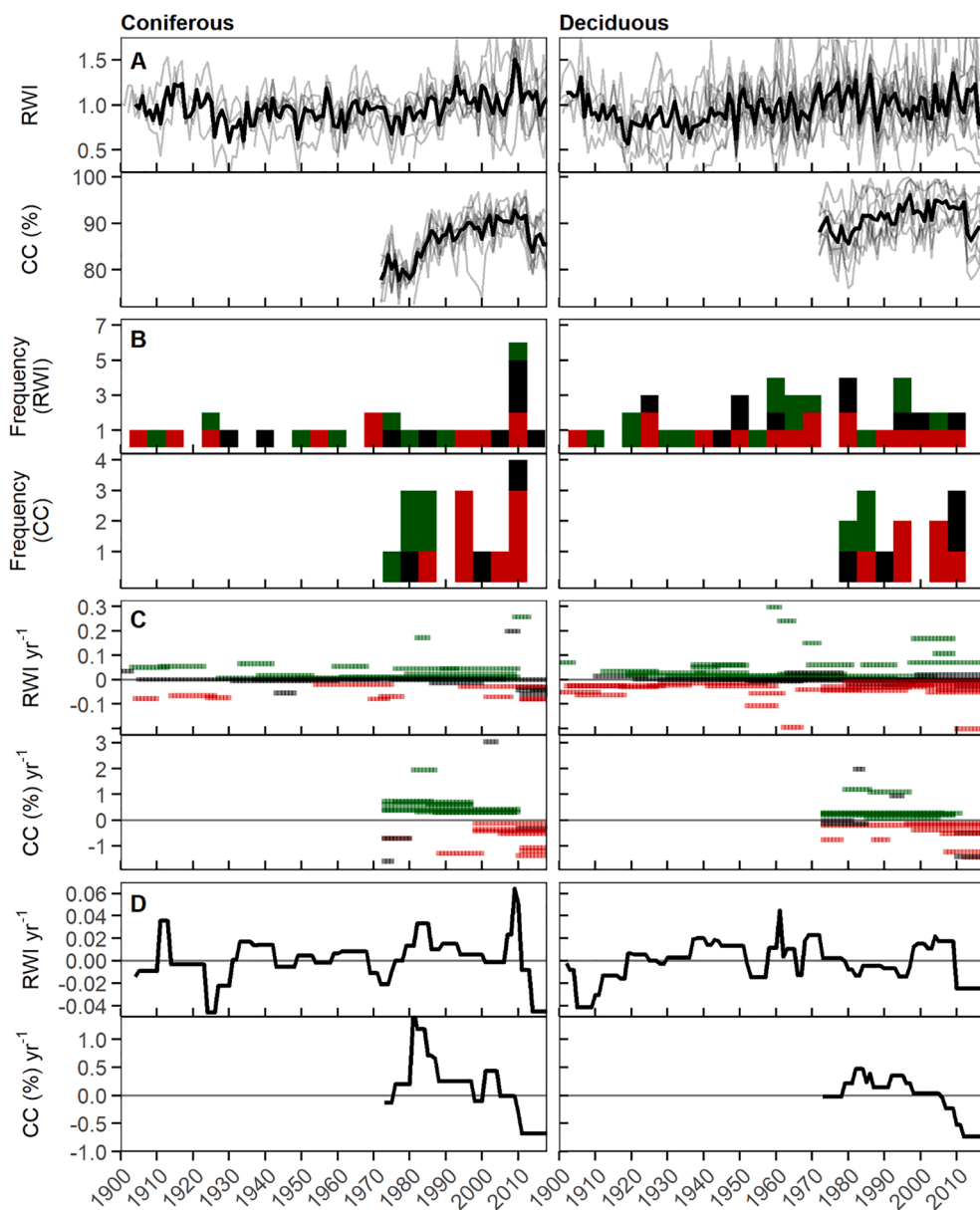


Fig. 8. Results from Figs. 7 and A6 with plots combined by chronology forest type (left: coniferous, right: deciduous). A. Input RWI and CC time-series. Thicker lines are the average. B. Frequency of breakpoints in 5-year bins. Red bars are breakpoints that precede declining segments, green bars precede increasing segments and black bars precede insignificant segments. C. Slope of increase-decline segments through time. For example, the first CC segment for site 01Tsu occurred from 1972 to 2010 at an increase of 0.41% per year. Colors are the same as Fig. 7. D. Average slope of all segments (i.e., from part C). (For interpretation of the references to color in this figure legend, the reader is referred to the web version of this article.)

Table 2

Forest type comparison of RWI and CC segmented regression slopes (Fig. 7, 8c-d) for 1983 and 2018. Slope direction is positive (+) or negative (-), with the percentage of the majority direction shown in parentheses (significant percentage in bold). For example, in 2018 7/8 (88%) of coniferous RWI slopes were negative and 3/8 (38%) were significantly negative. Magnitude is the average and standard deviation of the slopes.

Coniferous				
1983		2018		
	Direction (\pm)	Magnitude (yr^{-1})	Direction (\pm)	
RWI	+ (100/75%)	0.033 ± 0.055	- (88/38%)	-0.045 ± 0.025
CC (%)	+ (100/88%)	1.18 ± 1.30	- (100/88%)	-0.68 ± 0.43
Deciduous				
1983		2018		
	Direction (\pm)	Magnitude (yr^{-1})	Direction (\pm)	
RWI	- (67/42%)	-0.013 ± 0.019	- (75/50%)	-0.025 ± 0.061
CC (%)	+ (75/63%)	0.47 ± 0.69	- (100/75%)	-0.74 ± 0.51

identification of five decades of increase-decline trends. To do this, we incorporated recent advances in building spectrally consistent Landsat time-series across all sensors (MSS, TM, ETM+, OLI) with the LandsatLinkr framework (Fig. A1; Braaten et al., 2017). Landsat's higher spatial resolution allowed us to work in many small and fragmented forests (Fig. 3), where other sensors would not have been able to isolate the forest change signal. Other studies have taken advantage of Landsat to work in irregular forest landscapes (Dorman et al., 2015), but not in urban forests or to this degree of local landscape heterogeneity. Interestingly, in three of four multi-chronology sites (e.g., 02, 03, 10), Landsat time-series related significantly with one chronology, indicating the possibility of connection with individual species or genera within diverse stands.

In addition to their fragmented and heterogeneous nature, these are dense temperate forest sites where limiting factors are complex. For example, Seftigen et al. (2018) found that NDVI is driven by growing season climate in most Northern Hemisphere forests, but that eastern North America is an exception. As we will discuss, forest types and their differing connection to seasonal climate led to variation in connection with TCA-based CC. The dense canopy at our sites and the abundance of

NDVI-based comparisons led us to consider VIs that utilize additional wavelengths and are less likely to saturate in high-biomass settings (e.g., Sangüesa-Barreda et al., 2014). Comparisons with canopy variables derived from hemispherical photographs led to a strong relationship ($R^2 = 0.67^{***}$) between TCA and CC above 75% (Fig. A2), higher than other tested VIs. Ahmed et al. (2014) similarly found a strong relationship ($r = 0.86$) between TCA and Lidar-derived CC. TCA (which is highly correlated to NDVI) proves to be a useful VI for long-term forest change monitoring with Landsat in dense temperate forests.

4.2. Relationship variation by forest type

Across all chronologies, the average RWI-CC correlation was weak ($r = 0.16$) and highly variable, with our goal to better understand that variation (Figs. 4, 5). Despite this, more than half of sites had a significant relationship. Forest type most influenced correlations, with coniferous chronologies ($r = 0.35 \pm 0.18$) correlating significantly stronger than deciduous ($r = 0.03 \pm 0.25$) and especially maple. When reduced to averages (Fig. 8a) the difference increases (coniferous $r = 0.56^{**}$, deciduous $r = -0.27$). Even at the same location (site 10, Fig. 4), coniferous RWI related significantly with CC ($r = 0.55^*$), while deciduous RWI had a negative correlation ($r = -0.17$). Many broad-scale studies include tree-rings from temperate forests, including eastern North America, but have generally found weak and non-significant relationships there, especially at deciduous chronology sites (Babst et al., 2018; Bhuyan et al., 2017; Seftigen et al., 2018). The closer connection between coniferous chronologies and NDVI has been identified globally (Bhuyan et al., 2017; Kaufmann et al., 2008). More focused studies in temperate forests elsewhere have ranged in correlation and significance from weak (coniferous; Wang et al., 2020) to moderate (deciduous; Decuyper et al., 2020) to strong (coniferous; Correa-Díaz et al., 2019). Our Landsat-based results generally align with previous research using lower spatial resolution sensors but reveal local-scale forest type variation.

Differential response to seasonal temperature connects to the variation in correlation by forest type (Fig. 6a-b). CC, based on summer Landsat data, correlated most positively with June temperature (deciduous $r = 0.31 \pm 0.27$, coniferous $r = 0.44 \pm 0.15$). However, deciduous RWI correlated negatively with summer temperature (June-August $r = -0.32 \pm 0.22$). This means that temperature warming since 1980 (Fig. 2a-b) led to CC increase but stagnation and decline in deciduous RWI trends (Fig. 8, Table 2). There is evidence that coniferous TRWs relate to summer NDVI, while deciduous TRWs relate to spring or fall NDVI (Kaufmann et al., 2008), and we found that spring was the only season with a positive deciduous RWI-temperature correlation. The lower temporal resolution of Landsat, and lower data availability further back in time (especially in MSS period), combined with the speed of deciduous canopy growth in the spring or senescence in the fall make it difficult to build a long-term fall or spring VI time-series that avoids seasonality noise (Fig. 2b). It may be possible to build a better connection with deciduous tree-rings with higher temporal resolution sensors, but (as discussed) those have been extensively tested with mixed results. There were also disconnects between RWI and CC correlation with summer precipitation, but not by forest type (Fig. 6c-d).

Seasonal climate does not fully explain variations in the RWI-CC relationship. With few exceptions (e.g., deciduous RWI and summer temperature), RWI only correlates weakly with climate (r between -0.2 and 0.2) with few significant relationships (Fig. 6). Coniferous CC correlates more strongly with temperature than deciduous, with the bulk of significant relationships. These deciduous disconnects may also be attributable to difficulties quantifying gradual canopy change in dense deciduous canopies. Although TCA and CC relate strongly across forest types (Fig. A2), the relationship is much weaker at deciduous sites ($R^2 = 0.15$) compared to coniferous ($R^2 = 0.89^{**}$). It appears that even TCA (which connects better to CC than NDVI) can struggle to spectrally observe small CC changes in dense broadleaf foliage, likely manifesting

in a noisier time-series (e.g., site 02, Fig. 4). There may also be a larger biological disconnect for deciduous species, especially maple. Huang et al. (2014) modeled a connection between wood formation and canopy growth for boreal conifers, but we did not locate similar findings for relevant deciduous species.

RWI and CC increase-decline trends were remarkably similar, especially for coniferous chronologies, while deciduous only somewhat align since 2010. Throughout the overlap period and especially in the 1980s (strong increase period) and 2010s (strong decline period), coniferous RWI and CC trend in the same direction and at similar relative magnitudes in almost every case (Figs. 7, 8, Table 2). Others comparing multi-year trends have also been successful in finding consistent temporal patterns (Beck et al., 2011; Berner et al., 2011; Decuyper et al., 2020). Even deciduous RWI and CC are both declining in most cases in the 2010s, although not to the same consistency as coniferous and without the same alignment of breakpoints. In 2013 a major ice storm impacted this region, likely driving declines in RWI and especially CC (which steeply declines at the same time) where the damage remains visible at many sites (Decuyper et al., 2020). In Québec, Canada, Pisarcic et al. (2008) found that damaged sugar maple TRW from a major 1998 ice storm had not returned to pre-storm sizes in at least six years.

However, it is difficult to disentangle these declines from other factors. For example, coniferous RWI is also declining from a strong increase period in the late 2000s associated with above-average precipitation (Fig. 2c). Furthermore, EAB became a major presence in this area in the 2010s, and many of the sites we visited contained standing dead ash trees. EAB may decrease CC (ash canopy lost), but increase RWI (non-ash trees taking advantage of the decrease in competition) (e.g., Trotsiuk et al., 2018). We also do not have regular records on specific management practices undertaken at these sites, which may be especially influential at the two plantations (site 09, 13). Although the focus of this paper is on better understanding temporal connections between tree-rings and Landsat time-series across these diverse temperate stands, it would be useful to isolate these potentially contrasting disturbance and forest management signals from climate in the future.

4.3. Applied significance

Our main goal was to visit a variety of temperate forest types and settings and compare tree-rings with long-term Landsat time-series to better understand influencing factors (discussed above) and research utility (e.g., should remote sensing scientists working in these areas consider TRW as a validation tool?). Our results indicate that hemlock and cedar coniferous chronologies often significantly correlate with Landsat time-series, even in mixed forest stands (Figs. 3, 4). These sites were located across the urban-rural continuum, with Landsat's spatial resolution allowing for comparisons even in small and irregular forest stands (e.g., city parks). We assert that this type of analysis can be used to verify changes quantified by Landsat in urban forest stands, which have increased ecological importance (Roy et al., 2012). Commonly used validation methods, such as hemispherical photographs, forest inventories or Lidar, are useful but limited to specific locations and points in time. Aerial photography can validate over larger areas, but we are still limited to where high-resolution photographs have been collected in the past, especially farther back in time and in more remote areas. By comparison, TRWs provide a yearly measurement of forest productivity longer into the past than any satellite in any forest location without having to rely on past data collection in that area.

However, results in deciduous stands were less promising. With a few exceptions (e.g., 12Pop), deciduous chronologies had weak, and sometimes negative, correlations with CC (Fig. 4). We provided several explanations, including disconnects with summer temperature (Fig. 6a,b) and Landsat struggling to spectrally observe small changes in dense deciduous canopies. Our results suggest avoiding deciduous chronologies for validating long-term annual summer Landsat time-series. This is

true in most cases for other sensors with higher temporal resolutions (e.g., Bhuyan et al., 2017), meaning that the ‘deciduous disconnect’ remains an area of concern that should be further investigated. Beyond forest type, the history of the site should be considered. For example, disturbances that are expected to decrease both TRW and VIs (e.g., ice storms) may be useful for providing some confidence in results even if gradual or year-to-year change does not show a relationship.

5. Conclusion

In this study, we test the power of Landsat, with a 30 m spatial resolution and nearly 50-year history of spectrally consistent (summer) data, for combining with tree ring width and monitoring gradual canopy cover change in an urban–rural temperate forest. We found significant variation in correlation and contrasting increase-decline trends by forest type (i.e., coniferous vs. deciduous) between negative exponential detrended ring width index and Landsat-derived canopy cover, with significant relationships at nine of 20 chronologies at 16 sites. Coniferous chronologies relate more strongly with Landsat than deciduous, with maple being especially weak. Deciduous ring width’s negative response and canopy cover’s positive response to summer temperature warming, play a major role in this disconnect. The major 2013 ice storm appears to contribute to recent decline trends across forest types. The biological relationship between wood growth and canopy productivity is complicated and indirect, but useful for dendrochronologists and remote sensing scientists working with time-series in different environments. We hope that this multidisciplinary study leads researchers to consider the utility of the other data source and apply them to improve their results and understanding of long-term forest change.

CRediT authorship contribution statement

Mitchell T. Bonney: Conceptualization, Methodology, Formal analysis, Investigation, Writing – original draft, Writing – review & editing, Visualization. **Yuhong He:** Writing – review & editing, Supervision, Funding acquisition.

Declaration of Competing Interest

The authors declare that they have no known competing financial interests or personal relationships that could have appeared to influence the work reported in this paper.

Acknowledgments

The project is supported by the Natural Sciences and Engineering Research Council of Canada (NSERC) Discovery Program (RGPIN-386183) awarded to Yuhong He. This work was also financially supported by the Department of Geography, Geomatics and Environment and the Centre for Urban Environments at the University of Toronto Mississauga, the Natural Sciences and Engineering Research Council of Canada (NSERC) Postgraduate Scholarship, and the Mitacs Research Training Award awarded to Mitchell Bonney. We are grateful to Credit Valley Conservation, and especially Kelsey McNeill, for support and permission to conduct fieldwork. We also thank the City of Mississauga, City of Brampton, and the Town of Oakville. We thank Trevor Porter, Katherine Dearborn, Greg King, and Logan Berner for advice on dendrochronology and related statistics; Justin Braaten and Jody Vogeler for LandsatLinkr guidance; Phil Rudz for providing field equipment and expertise; and field and lab assistants Esther Kaye, Zoe Bedford, Monique Dosanjh, and Ali Al Wafi.

Appendix A. Supplementary material

Supplementary data to this article can be found online at <https://doi.org/10.1016/j.jag.2021.102523>.

References

- Ahmed, O.S., Franklin, S.E., Wulder, M.A., 2014. Interpretation of forest disturbance using a time series of Landsat imagery and canopy structure from airborne lidar. Canadian J. Remote Sens. 39 (6), 521–542.
- Babst, F., Bodesheim, P., Charney, N., Friend, A.D., Girardin, M.P., Klesse, S., Moore, D.J.P., Seftigen, K., Björklund, J., Bouriaud, O., Dawson, A., DeRose, R.J., Dietze, M.C., Eckes, A.H., Enquist, B., Frank, D.C., Mahecha, M.D., Poulter, B., Record, S., Trouton, V., Turton, R.H., Zhang, Z., Evans, M.E.K., 2018. When tree rings go global: Challenges and opportunities for retrospective insight. Quat. Sci. Rev. 197, 1–20.
- Babst, F., Bouriaud, O., Papale, D., Gielen, B., Janssens, I.A., Nikinmaa, E., Ibrom, A., Wu, J., Bernhofer, C., Köstner, B., Grünwald, T., Seufert, G., Ciais, P., Frank, D., 2013. Above-ground woody carbon sequestration measured from tree rings is coherent with net ecosystem productivity at five eddy-covariance sites. New Phytol. 201 (4), 1289–1303.
- Babst, F., Esper, J., Parlow, E., 2010. Landsat TM/ETM+ and tree-ring based assessment of spatiotemporal patterns of the autumnal moth (*Epirrita autumnata*) in northernmost Fennoscandia. Remote Sens. Environ. 114 (3), 637–646.
- Banskota, A., Kayastha, N., Falkowski, M.J., Wulder, M.A., Froese, R.E., White, J.C., 2014. Forest monitoring using Landsat time-series data: a review. Canadian J. Remote Sens. 40 (5), 362–384.
- Beck, P.S.A., Juday, G.P., Alix, C., Barber, V.A., Winslow, S.E., Sousa, E.E., Goetz, S.J., 2011. Changes in forest productivity across Alaska consistent with biome shift. Ecol. Lett. 14, 373–379.
- Berner, L.T., Beck, P.S.A., Bunn, A.G., Lloyd, A.H., Goatz, S.J., 2011. High-latitude tree growth and satellite vegetation indices: correlations and trends in Russia and Canada (1982–2008). J. Geophys. Res. 116, G01015.
- Bhuyan, U., Zang, C., Vicente-Serrano, S., Menzel, A., 2017. Exploring relationships among tree-ring growth, climate variability, and seasonal leaf activity on varying timescales and spatial resolutions. Remote Sensing 9 (6), 526. <https://doi.org/10.3390/rs9060526>.
- Bonney, M.T., Danby, R.K., Treitz, P.M., 2018. Landscape variability of vegetation change across the forest to tundra transition of central Canada. Remote Sens. Environ. 217, 18–29.
- Braaten, J.D., Cohen, W.B., Yang, Z., 2017. LandsatLinkr. Zenodo. <https://doi.org/10.5281/zenodo.807733> (accessed 16 September 2020).
- Braaten, J.D., Cohen, W.B., Yang, Z., 2015. Automated cloud and shadow identification in Landsat MSS imagery for temperate ecosystems. Remote Sens. Environ. 169, 128–138.
- Brehaut, L., Danby, R.K., 2018. Inconsistent relationships between annual tree ring widths and satellite-measured NDVI in a mountainous subarctic environment. Ecol. Ind. 91, 698–711.
- Bronaugh, D., Werner, A., 2019. zyp: Zhang + Yue-Pilon Trends Package. R package version 0.10-1.1. <https://CRAN.R-project.org/package=zyp>.
- Bunn, A.G., 2008. A dendrochronology program library in R (dplR). Dendrochronologia 26 (2), 115–124.
- Bunn, A.G., 2010. Statistical and visual crossdating in R using the dplR library. Dendrochronologia 28 (4), 251–258.
- Buras, A., 2017. A comment on the Expressed Population Signal. Dendrochronologia 44, 130–132.
- Chavez, P.S., 1996. Image-based atmospheric corrections-revisited and improved. Photogramm. Eng. Remote Sens. 62 (9), 1025–1035.
- Chavez, P.S., 1988. An improved dark-object subtraction technique for atmospheric scattering correction of multispectral data. Remote Sens. Environ. 24 (3), 459–479.
- Correa-Díaz, A., Silva, L.C.R., Horwath, W.R., Gómez-Guerrero, A., Vargas-Hernández, J., Villanueva-Díaz, J., Velázquez-Martínez, A., Suárez-Espinoza, J., 2019. Linking remote sensing and dendrochronology to quantify climate-induced shifts in high-elevation forests over space and time. J. Geophys. Res. Biogeosci. 124 (1), 166–183.
- Coulthard, B.L., Touchan, R., Anchukaitis, K.J., Meko, D.M., Sivrikaya, F., 2017. Tree growth and vegetation activity at the ecosystem-scale in the eastern Mediterranean. Environ. Res. Lett. 12 (8), 084008. <https://doi.org/10.1088/1748-9326/aa7b26>. [dataset] Credit Valley Conservation (CVC), 2019. Ecological land classification.
- Crist, E.P., 1985. A TM tasseled cap equivalent transformation for reflectance factor data. Remote Sens. Environ. 17 (3), 301–306.
- Davies, R.B., 2002. Hypothesis testing when a nuisance parameter is present only under the alternative: linear model case. Biometrika 89 (2), 484–489.
- Dawdy, D.R., Matalas, N.C., 1964. Statistical and probability analysis of hydrological data, part III: analysis of variance, covariance and time series. In: Chow, V.T. (Ed.), Handbook of Applied Hydrology, a Compendium of Water-Resources Technology. McGraw-Hill, New York, pp. 8.68–8.90.
- Decuyper, M., Chávez, R.O., Ćufar, K., Estay, S.A., Clevers, J.G.P.W., Prislanić, P., Grigar, J., Crepinšek, Z., Merela, M., de Luis, M., Notivoli, R.S., del Castillo, E.M., Rozendaal, D.M.A., Bongers, F., Herold, M., Sass-Klaassen, U., 2020. Spatio-temporal assessment of beech growth in relation to climate extremes in Slovenia – An integrated approach using remote sensing and tree-ring data. Agric. For. Meteorol. 287, 107925. <https://doi.org/10.1016/j.agrformet.2020.107925>.
- Dorman, M., Svoray, T., Perevolotsky, A., Moshe, Y., Sarris, D., 2015. What determines tree mortality in dry environments? A multi-perspective approach. Ecol. Appl. 25 (4), 1054–1071.
- Fritts, H.C., 2001. Tree Rings and Climate. Blackburn. ISBN-13: 978-1-930665-39-2.
- Hamed, K.H., Rao, A.R., 1998. A modified Mann-Kendall trend test for autocorrelated data. J. Hydrol. 204 (1–4), 182–196.
- Huang, J.-G., Deslauriers, A., Rossi, S., 2014. Xylem formation can be modeled statistically as a function of primary growth and cambium activity. New Phytol. 203 (3), 831–841.

- Kaufmann, R.K., D'Arrigo, R.D., Paletta, L.F., Tian, H.Q., Matt Jolly, W., Myneni, R.B., 2008. Identifying climatic controls on ring width: the timing of correlations between tree rings and NDVI. *Earth Interact* 12 (14).
- Kendall, M.G., 1975. Rank correlation measures. Charles Griffin, London, p. 15.
- Kennedy, R.E., Cohen, W.B., 2003. Automated designation of tie-points for image-to-image coregistration. *Int. J. Remote Sens.* 24 (17), 3467–3490.
- Larsson, L.Å., 2019. CDendro & CooRecorder software dendrochronology measurements and dating, version 9.3.1. <http://www.cybis.se/forfun/dendro/>.
- Leblanc, S.G., 2008. DHP-TRACWin Manual. Natural Resources Canada, Canada Centre for Remote Sensing.
- Ma, Q., Su, Y., Luo, L., Li, L.e., Kelly, M., Guo, Q., 2018. Evaluating the uncertainty of Landsat-derived vegetation indices in quantifying forest fuel treatments using bi-temporal LiDAR data. *Ecol. Ind.* 95, 298–310.
- Mann, H.B., 1945. Nonparametric tests against trend. *Econometrica: J. Econ. Soc.* 13 (3), 245. <https://doi.org/10.2307/1907187>.
- Masek, J.G., Vermote, E.F., Saleous, N.E., Wolfe, R., Hall, F.G., Huemmrich, K.F., Gao, F., Kutler, J., Lim, T.-K., 2006. A Landsat surface reflectance dataset for North America, 1990–2000. *IEEE Geosci. Remote Sens. Lett.* 3 (1), 68–72.
- Mekis, É., Vincent, L.A., 2011. An overview of the second generation adjusted daily precipitation dataset for trend analysis in Canada. *Atmos. Ocean* 49 (2), 163–177.
- Mississauga Parks & Forestry, 2020. Forestry pest & disease management: Emerald ash borer. City of Mississauga. <http://www.mississauga.ca/portal/residents/parks-emerald-ash-borer> (accessed 11 September 2020).
- Muggeo, V.M., 2008. Segmented: an R package to fit regression models with broken-line relationships. *R News* 8, 20–25.
- Muggeo, V.M., 2020. Selecting number of breakpoints in segmented regression: implementation in the R package segmented. Technical report. DOI: 10.13140/RG.2.2.12891.39201.
- Patakanuri, S.K., O'Brien, N., 2020. modifieddmk: Modified versions of Mann Kendall and Spearman's Rho Trend Tests. R package version 1.5.0, <https://CRAN.R-project.org/package=modifieddmk>.
- Pearl, J.K., Keck, J.R., Tintor, W., Siekacz, L., Herrick, H.M., Meko, M.D., Pearson, C.L., 2020. New frontiers in tree-ring research. *The Holocene* 30 (6), 923–941.
- Pflugmacher, D., Cohen, W.B., E. Kennedy, R., 2012. Using Landsat-derived disturbance history (1972–2010) to predict current forest structure. *Remote Sens. Environ.* 122, 146–165.
- Pisaric, M.F.J., King, D.J., MacIntosh, A.J.M., Bemrose, R., 2008. Impact of the 1998 ice storm on the health and growth of sugar maple (*Acer saccharum* Marsh.) dominated forests in Gatineau Park, Quebec. *J. Torrey Bot. Soc.* 135 (4), 530–539.
- Powell, S.L., Cohen, W.B., Healey, S.P., Kennedy, R.E., Moisen, G.G., Pierce, K.B., Ohmann, J.L., 2010. Quantification of live aboveground forest biomass dynamics with Landsat time-series and field inventory data: a comparison of empirical modeling approaches. *Remote Sens. Environ.* 114 (5), 1053–1068.
- R Core Team, 2013. R: A language and environment for statistical computing. R Foundation for Statistical Computing, Vienna, Austria <https://www.r-project.org/> (accessed 16 September 2020).
- Rodman, K.C., Andrus, R.A., Veblen, T.T., Hart, S.J., 2021. Disturbance detection in Landsat time series is influenced by tree mortality agent and severity, not by prior disturbance. *Remote Sens. Environ.* 254, 112244. <https://doi.org/10.1016/j.rse.2020.112244>.
- Roy, S., Byrne, J., Pickering, C., 2012. A systematic quantitative review of urban tree benefits, costs, and assessment methods across cities in different climatic zones. *Urban For. Urban Greening* 11 (4), 351–363.
- Sangüesa-Barreda, G., Camarero, J.J., García-Martín, A., Hernández, R., de la Riva, J., 2014. Remote-sensing and tree-ring based characterization of forest defoliation and growth loss due to the Mediterranean pine processionary moth. *For. Ecol. Manage.* 320, 171–181.
- Seftigen, K., Frank, D.C., Björklund, J., Babst, F., Poulter, B., 2018. The climate drivers of normalized difference vegetation index and tree-ring-based estimates of forest productivity are spatially coherent but temporally decoupled in Northern Hemispheric forests. *Glob. Ecol. Biogeogr.* 27, 1352–1365.
- Sen, P.K., 1968. Estimates of the regression coefficient based on Kendall's tau. *J. Am. Stat. Assoc.* 63 (324), 1379–1389.
- Speer, J.H., 2010. Fundamentals of Tree-Ring Research. University of Arizona Press, Tucson, Arizona.
- Tei, S., Sugimoto, A., 2018. Time lag and negative responses of forest greenness and tree growth to warming over circumboreal forests. *Glob. Change Biol.* 24 (9), 4225–4237.
- Theil, H., 1950. A rank-invariant method of linear and polynomial regression analysis I, II and III. Proceedings, Koninklijke Nederlandse Academie van Wetenschappen, 53, pp. 386–392, 521–525, 1397–1412.
- Trotsiuk, V., Pederson, N., Druckenbrod, D.L., Orwig, D.A., Bishop, D.A., Barker-Plotkin, A., Fraver, S., Martin-Benito, D., 2018. Testing the efficacy of tree-ring methods for detecting past disturbances. *For. Ecol. Manage.* 425, 59–67.
- Vermote, E., Justice, C., Claverie, M., Franch, B., 2016. Preliminary analysis of the performance of the Landsat 8/OLI land surface reflectance product. *Remote Sens. Environ.* 185, 46–56.
- Vicente-Serrano, S., Camarero, J.J., Olano, J.M., Martín-Hernández, N., Peña-Gallardo, M., Tomás-Burguera, M., El Kenawy, A., 2016. Diverse relationship between forest growth and the Normalized Difference Vegetation Index at a global scale. *Remote Sens. Environ.* 187, 14–29.
- Vincent, L.A., Hartwell, M.M., Wang, X.L., 2020. A third generation of homogenized temperature for trend analysis and monitoring changes in Canada's climate. *Atmos. Ocean* 58 (3), 173–191.
- Vogeler, J.C., Braaten, J.D., Slesak, R.A., Falkowski, M.J., 2018. Extracting the full value of the Landsat archive: Inter-sensors harmonization for the mapping of Minnesota forest canopy cover (1973–2015). *Remote Sens. Environ.* 209, 363–374.
- Wang, Z., Lyu, L., Liu, W., Liang, H., Huang, J., Zhang, Q.-B., 2021. Topographic patterns of forest decline as detected from tree rings and NDVI. *Catena* 198, 105011. <https://doi.org/10.1016/j.catena.2020.105011>.
- Wigley, T.M.L., Briffa, K.R., Jones, P.D., 1984. On the average value of correlated time series, with applications in dendroclimatology and hydrometeorology. *J. Climate Appl. Meteorol.* 23 (2), 201–213.
- Xu, P., Fang, W., Zhou, T., Zhao, X., Luo, H., Hendrey, G., Yi, C., 2019. Spatial upscaling of tree-ring-based forest response to drought with satellite data. *Remote Sensing* 11 (20), 2344. <https://doi.org/10.3390/rs11202344>.
- Zhou, Y., Yi, Y., Jia, W., Cai, Y., Yang, W., Li, Z., 2017. Applying dendrochronology and remote sensing to explore climate-drive in montane forests over space and time. *Quat. Sci. Rev.* 237, 106292.
- Zhu, Z., Wang, S., Woodcock, C.E., 2015. Improvement and expansion of the Fmask algorithm: cloud, cloud shadow, and snow detection for Landsats 4–7, 8, and Sentinel 2 images. *Remote Sens. Environ.* 159, 269–277.